Mechanistic mathematical model of polarity in yeast

Natasha S. Savage[a], Anita T. Layton[b], and Daniel J. Lew[a]
[a]Department of Pharmacology and Cancer Biology, Duke University Medical Center, Durham, NC 27710; [b]Department of Mathematics, Duke University, Durham, NC 27708

ABSTRACT **The establishment of cell polarity involves positive-feedback mechanisms that concentrate polarity regulators, including the conserved GTPase Cdc42p, at the "front" of the polarized cell. Previous studies in yeast suggested the presence of two parallel positive-feedback loops, one operating as a diffusion-based system, and the other involving actin-directed trafficking of Cdc42p on vesicles. F-actin (and hence directed vesicle traffic) speeds fluorescence recovery of Cdc42p after photobleaching, suggesting that vesicle traffic of Cdc42p contributes to polarization. We present a mathematical modeling framework that combines previously developed mechanistic reaction-diffusion and vesicle-trafficking models. Surprisingly, the combined model recapitulated the observed effect of vesicle traffic on Cdc42p dynamics even when the vesicles did not carry significant amounts of Cdc42p. Vesicle traffic reduced the concentration of Cdc42p at the front, so that fluorescence recovery mediated by Cdc42p flux from the cytoplasm took less time to replenish the bleached pool. Simulations in which Cdc42p was concentrated into vesicles or depleted from vesicles yielded almost identical predictions, because Cdc42p flux from the cytoplasm was dominant. These findings indicate that vesicle-mediated delivery of Cdc42p is not required to explain the observed Cdc42p dynamics, and raise the question of whether such Cdc42p traffic actually contributes to polarity establishment.**

Monitoring Editor
Leah Edelstein-Keshet
University of British Columbia

Received: Oct 6, 2011
Revised: Mar 7, 2012
Accepted: Mar 14, 2012

INTRODUCTION

The spontaneous emergence of spatial patterns from homogeneous starting conditions has long fascinated theoreticians as well as biologists (Turing, 1952; Gierer and Meinhardt, 1972). In recent years, the growing availability of detailed molecular information has stimulated attempts to develop increasingly realistic mathematical models of biological pattern formation (Jilkine and Edelstein-Keshet, 2011). One particularly simple and experimentally tractable instance of such pattern formation is the establishment of cell polarity in the budding yeast *Saccharomyces cerevisiae*. This process is normally biased to occur at prespecified locations (Chant and Pringle, 1995) but can occur spontaneously at random locations (referred to as "symmetry breaking") when bud-site-selection genes are ablated (Bender and Pringle, 1989; Chant and Herskowitz, 1991). Symmetry-breaking polarization is thought to rely on two parallel, positive-feedback loops that activate and concentrate the conserved polarity regulator Cdc42p at the site destined to become the "front" of the polarized cell (Wedlich-Soldner *et al.*, 2004; Slaughter *et al.*, 2009).

The first feedback loop is a diffusion-based system that represents a specific case of a more general "substrate depletion" class of pattern formation models (Meinhardt and Gierer, 1974). Cdc42p is a Rho-family GTPase that is enriched on the cytoplasmic face of cellular membranes (particularly the plasma membrane) due to C-terminal prenylation. At the membrane, Cdc42p can interconvert between GDP- and GTP-bound forms, stimulated by guanine nucleotide exchange factors (GEFs) or GTPase-activating proteins (GAPs; Figure 1A, red arrows). The GTP-bound form can bind to a cytoplasmic complex, assembled by the scaffold protein Bem1p, that contains the GEF Cdc24p (Figure 1A, green arrows). This complex can provide positive feedback in that by recruiting the complex, GTP-Cdc42 promotes local generation of more GTP-Cdc42p (Kozubowski *et al.*, 2008). Because of this, a small stochastic increase in the local GTP-Cdc42p concentration at a random location can lead to the

This article was published online ahead of print in MBoC in Press (http://www.molbiolcell.org/cgi/doi/10.1091/mbc.E11-10-0837) on March 21, 2012.

Address correspondence to: Daniel J. Lew (daniel.lew@duke.edu).

Abbreviations used: FRAP, fluorescence recovery after photobleaching; GAP, GTPase activating protein; GDI, guanine nucleotide dissociation inhibitor; GEF, guanine nucleotide exchange factor; GFP, green fluorescent protein; v-SNARE, vesicle soluble *N*-ethylmaleimide-sensitive factor attachment protein receptor.

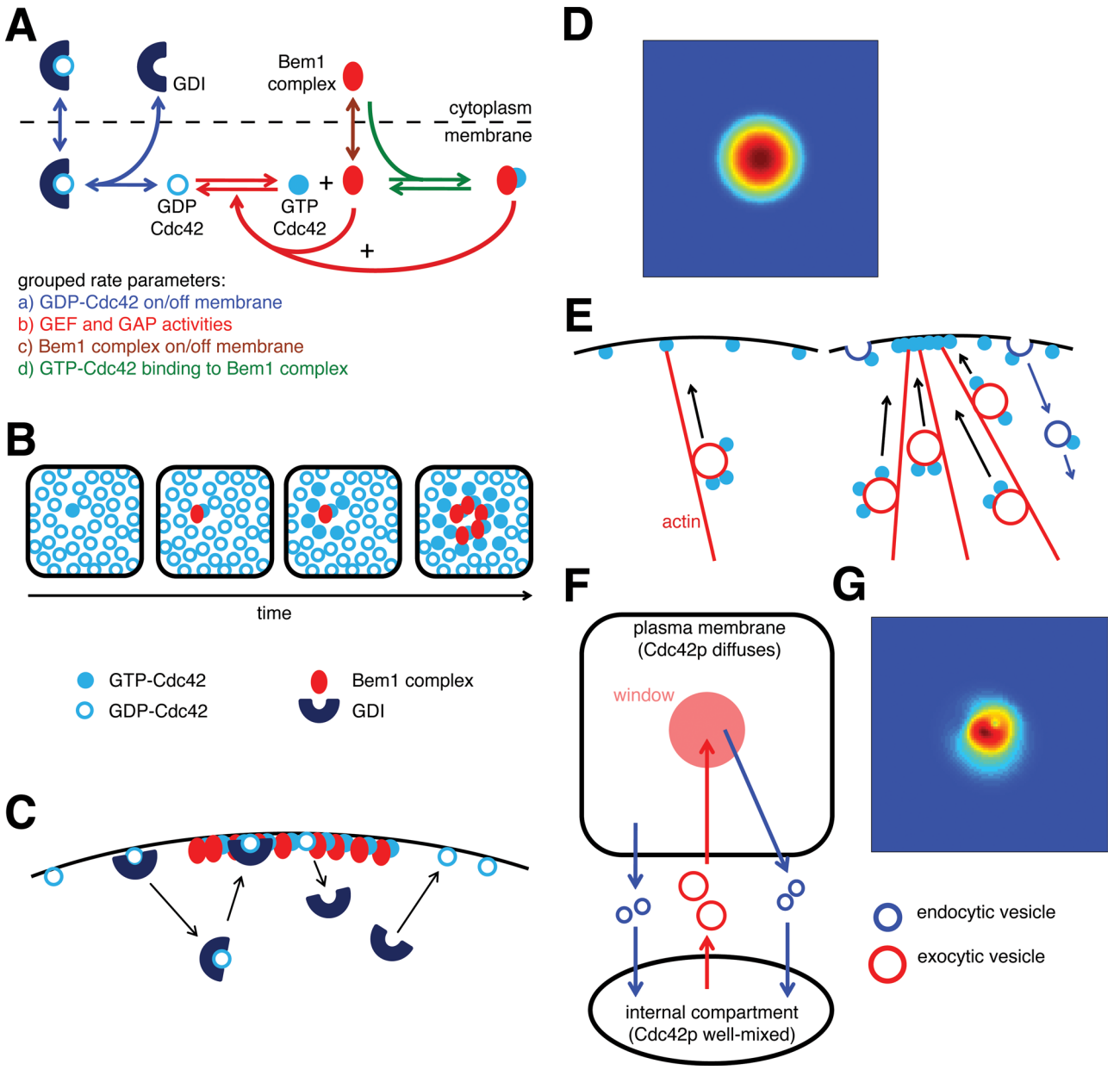

FIGURE 1: Cdc42p polarization via reaction-diffusion and vesicle-trafficking mechanisms. (A) Schematic of the reaction-diffusion model. +,positive feedback. (B) Positive feedback "grows" a cluster of GTP-Cdc42p. Stochastically arising GTP-Cdc42p recruits Bem1p complexes from the cytoplasm, promoting GTP loading of neighboring Cdc42p, and hence more Bem1p recruitment. (C) Cytoplasmic delivery of GDP-Cdc42 to the polarity patch via GDI. GDI extracts GDP-Cdc42p from the membrane to the cytoplasm, and returns it to the membrane. If GDI delivers GDP-Cdc42 to the polarity patch, Cdc42 becomes GTP-bound and thus protected from GDI removal, so the GDI mediates a net transfer of Cdc42p from outside to inside the cluster. (D) The square represents the plasma membrane, and the color indicates Cdc42p concentration (red, high; blue, low). A simulation of the scheme shown in (A) combined with diffusion was initiated with a small GTP-Cdc42p stimulus in the center of the membrane and developed the steady-state Cdc42p distribution shown. (E) Actin-mediated feedback loop. Cdc42p at the plasma membrane can nucleate an actin cable, which delivers vesicles carrying more Cdc42p to that site. The delivered Cdc42p can nucleate more actin cables, which deliver more vesicles containing Cdc42p, growing a cluster of Cdc42p. Endocytosis (blue arrows) returns Cdc42p to internal pools before it diffuses too far from the cluster. (F) Schematic of the vesicle-trafficking model. (G) A simulation of the scheme shown in (F) with traffic of vesicles carrying concentrated Cdc42p to/from a small central window yielded a fluctuating but polarized Cdc42p distribution (snapshot shown).

growth of a cluster of GTP-Cdc42p at the membrane (Johnson *et al.*, 2011; Figure 1B).

The GDP-bound form of Cdc42p can bind to a cytoplasmic guanine nucleotide dissociation inhibitor (GDI), and the GDI-Cdc42p complex can exchange between membrane and cytosol (Johnson *et al.*, 2009; Figure 1A, blue arrows). This reaction enables the local buildup of Cdc42p, as GDP-Cdc42p delivered to the cluster from the cytoplasm is quickly converted to GTP-Cdc42p by the local

GEF-containing Bem1p complexes and can no longer be removed by GDI (Johnson *et al.*, 2011; Figure 1C). Diffusion of membrane-bound proteins is slow, so newly generated GTP-Cdc42p tends to stay localized, whereas diffusion of cytoplasmic complexes is fast, so Bem1p and Cdc42p-GDI complexes from all over the cell can be rapidly captured by a growing cluster of GTP-Cdc42p (Figure 1C).

Goryachev and colleagues developed a mathematical model of this system using eight reaction-diffusion equations (Goryachev and Pokhilko, 2008). They showed that the uniform Cdc42p steady state exhibits Turing-type instability to spatial perturbation, evolving to a stable polarized distribution of Cdc42p. With parameter value estimates based on in vitro assays (Howell *et al.*, 2009), the model develops the polarized Cdc42p distribution shown in Figure 1D at steady state. Although the polarized Cdc42p distribution is stable, individual Cdc42p molecules cycle rapidly in and out of the polarization site, both in the model (Goryachev and Pokhilko, 2008) and in yeast cells (Wedlich-Soldner *et al.*, 2004). This model captures many features of yeast polarity establishment, but it does not explain experimental observations that the polarity cluster sometimes appears to move or disappear (Wedlich-Soldner *et al.*, 2004; Ozbudak *et al.*, 2005; Howell *et al.*, 2009, 2012), suggesting the model is incomplete. We prefer it to more abstract models, because it allows a more direct comparison with experimental data. Recycling of Cdc42p in all of these models requires a cytoplasmic Cdc42p species that is thought to be GDI-bound. However, the deletion of *RDI1* (the only GDI homologue) in yeast cells does not greatly impair polarity, although it does slow Cdc42p recycling considerably (Slaughter *et al.*, 2009). Thus, either there must be additional routes to traffic Cdc42p through the cytoplasm (Johnson *et al.*, 2011), or a vesicular recycling pathway must act in parallel, as discussed below.

The second feedback loop relies on actin-mediated trafficking of vesicles carrying Cdc42p (Wedlich-Soldner *et al.*, 2003). GTP-Cdc42p activates formins to nucleate polymerization of actin filaments, which are then assembled into linear actin cables with plus ends located at the polarization site (Pruyne *et al.*, 2004). Type V myosins deliver secretory vesicles toward the polarization site along the actin cables. Cdc42p is present on secretory vesicles (Orlando *et al.*, 2011) and is thereby delivered to the polarization site, potentially serving to concentrate Cdc42p at that site. Thus, a stochastic actin nucleation event at a random cortical site could lead to delivery of Cdc42p to that site, leading to further actin nucleation and vesicle delivery in a positive-feedback loop that could underlie spontaneous polarization (Figure 1E).

The second feedback loop is not necessary for polarization, because yeast cells can break symmetry in the absence of F-actin (Irazoqui *et al.*, 2003). It has been argued that the presence of both loops enhances the robustness of polarity establishment (Wedlich-Soldner and Li, 2004; Brandman *et al.*, 2005). However, the original observations that inspired the vesicle-trafficking feedback concept were obtained in an artificial system involving overexpression of a GTP-locked mutant form of Cdc42p (Wedlich-Soldner *et al.*, 2003). Because this mutant causes cell lysis and is incapable of polarizing at near-endogenous levels of expression (Irazoqui *et al.*, 2003), those observations are subject to alternative interpretations (Johnson *et al.*, 2011), and the validity of this feedback pathway remains controversial. In particular, it is still not clear whether vesicle traffic delivers sufficient Cdc42p to enable polarization by this mechanism.

Measurements of fluorescence recovery after photobleaching (FRAP) have provided quantitative data on the dynamics of green fluorescent protein (GFP)-Cdc42p recycling in vivo (Slaughter *et al.*, 2009). These data indicated that Cdc42p dynamics in latrunculin-treated cells (lacking F-actin and hence directed vesicle traffic) were slower than in untreated cells (recovery $t_{1/2} \approx 4$ s with actin and $t_{1/2} \approx 6$ s without actin). Similarly, slower Cdc42p FRAP dynamics were detected in mutants that impaired endocytosis (Slaughter *et al.*, 2009; Orlando *et al.*, 2011). These data were interpreted in the context of a mathematical model for Cdc42p redistribution that assumed additive fluxes of Cdc42p to the polarization site were provided by GDI delivery from the cytoplasm and by vesicle trafficking. After estimating parameters by fitting the FRAP data, the model produced realistic simulated Cdc42p distributions (Slaughter *et al.*, 2009), providing support for the founding assumptions.

The model discussed above incorporated fluxes of Cdc42p from internal pools toward a "window" representing the polarization site in the plasma membrane, and back to the internal compartment. However, the model did not consider fluxes of the membranes that carry Cdc42p. The validity of this simplifying assumption was recently challenged (Layton *et al.*, 2011) on the basis that the "membrane-free" formulation of Cdc42p fluxes means that *all* Cdc42p traffic to the window will concentrate Cdc42p at that site, no matter how little Cdc42p might be present on the vesicles. However, if the concentration of Cdc42p on vesicles is lower than that in the window, the actual effect of vesicle delivery would be to dilute Cdc42p at the polarization site, and thereby perturb (rather than maintain) polarization.

Layton and colleagues (Layton *et al.*, 2011) then developed a mathematical model that retained many features of the Slaughter model but explicitly included stochastic traffic of vesicles containing both membrane and Cdc42p between the internal compartment and the plasma membrane (Figure 1F). In this model, secretory vesicles (Figure 1F, red) budding from a well-mixed endo-membrane system are directed to a central "window," where they fuse with the plasma membrane. Endocytic vesicles (Figure 1F, blue) bud off from the plasma membrane and fuse with the endo-membrane system. The precise locations of vesicle fusion and budding events were determined by probabilistic rules. Vesicle sizes were estimated based on electron microscopy (Novick *et al.*, 1980; Prescianotto-Baschong and Riezman, 1998), and rates of vesicle traffic were estimated based on visualization of individual endocytic events in living cells (Kaksonen *et al.*, 2003). With this model, it became apparent that the Cdc42p distribution developed by vesicle traffic would be critically dependent on whether or not Cdc42p was actively concentrated into forming endocytic and exocytic vesicles (Layton *et al.*, 2011).

The actual behavior of Cdc42p during vesicle biogenesis is unknown. Modeling suggested that if Cdc42p were to behave like some integral membrane proteins (e.g., vesicle soluble *N*-ethylmaleimide-sensitive factor attachment protein receptors [v-SNAREs]), which are actively concentrated into both secretory and endocytic vesicles, then vesicle trafficking could in principle maintain a polarized Cdc42p distribution at the plasma membrane, as illustrated in Figure 1G. However, if vesicles simply carried Cdc42p at the same concentration as that of the source membrane ("bulk traffic"), then even highly polarized vesicle traffic would not yield a polarized Cdc42p distribution. This was true even if Cdc42p was concentrated into exocytic vesicles but not into endocytic vesicles, and in these cases, vesicle traffic would dissipate, rather than reinforce, polarity (Layton *et al.*, 2011).

We reasoned that revisiting the FRAP experiments (Slaughter *et al.*, 2009) using model simulations incorporating both the reaction-diffusion and vesicle-trafficking mechanisms should offer insight into the contribution of vesicle trafficking to Cdc42p polarization, potentially helping to distinguish whether or not vesicles mediate a significant flux of concentrated Cdc42p. We present mechanistic

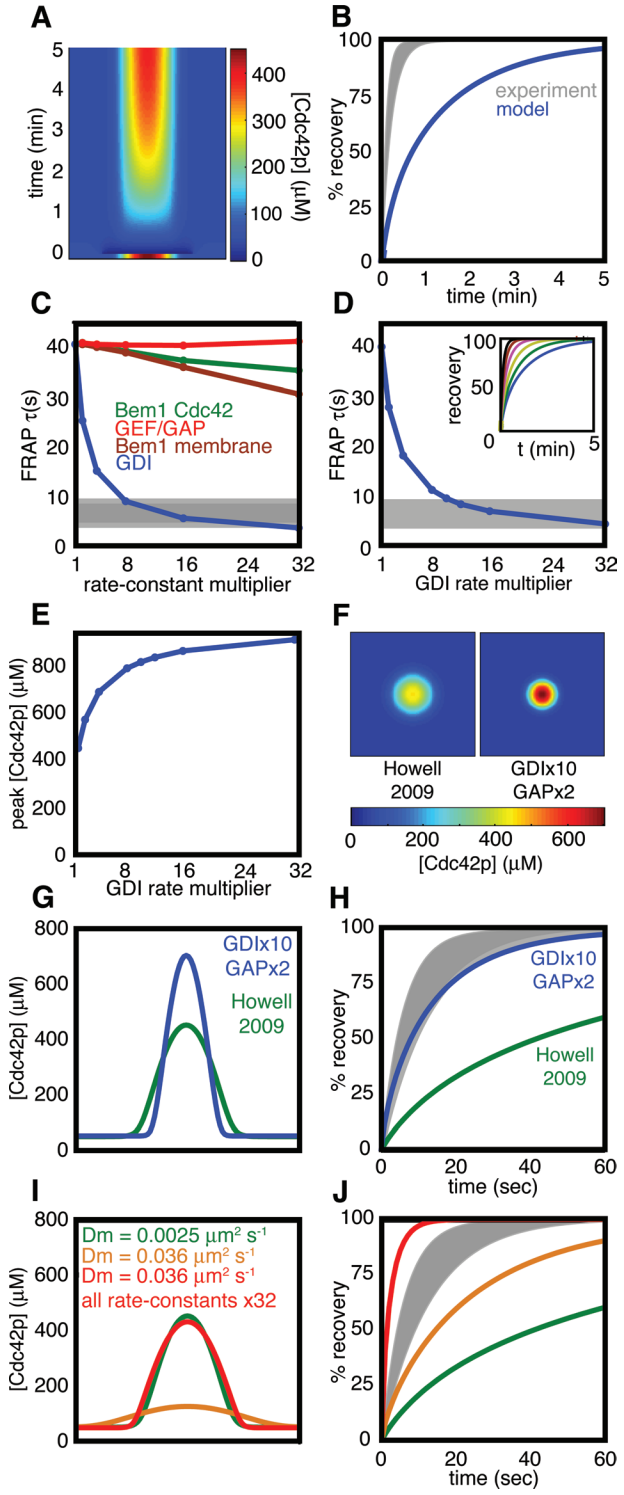

FIGURE 2: Comparison of simulated and experimental FRAP in latrunculin-treated cells. (A) Kymograph of a simulated FRAP experiment. A slice through the center of the plasma membrane (*x*-axis) is plotted against time (*y*-axis). The starting condition is the steady state (Figure 1D), and the dark blue at time zero indicates where the Cdc42p in the polarized spot was "bleached." Recovery of unbleached Cdc42p reveals the dynamic behavior of the model steady state. (B) Plot of the amount of unbleached Cdc42p in the polarization site from the simulation (blue) compared with experimental data from latrunculin-treated cells (gray zone = mean ± SD) from Slaughter *et al.* (2009). (C) Simulations of FRAP experiments varying model parameter sets (color as in Figure 1A, both forward and reverse rate constants multiplied by the same factor, simulated on a one-dimensional cell perimeter). τ, time to 50% simulated FRAP recovery; gray bar, mean ± SD for τ in latrunculin-treated cells (Slaughter *et al.*, 2009). (D) Simulations varying GDI rate constants on a two-dimensional membrane. Inset, FRAP dynamics for increasing GDI rates plotted as in (B). (E) Effect of increasing GDI rate constants on the peak Cdc42p concentration. (F) Comparison of steady-state Cdc42p distribution using previous (Howell *et al.*, 2009) vs. adjusted parameters. (G) The Cdc42p concentration profiles from (F) shown in cross-section. (H) Simulated FRAP kinetics using the new vs. old parameters, compared with the experimental FRAP. (I) Comparison of concentration profiles using diffusion constant 0.0025 μm²/s (green) or 0.036 μm²/s (gold). Adjusting all reaction rate constants to be 32× faster narrows the fast-diffusion peak (red). (J) Simulated FRAP kinetics for the peak profiles in (I).

mathematical models that combine the previous Goryachev and Layton formulations, yielding several unexpected findings (Goryachev and Pokhilko, 2008; Layton *et al.*, 2011). In particular, the combined model shows that vesicle traffic can have a net polarity-perturbing effect, even if Cdc42p is assumed to traffic like a v-SNARE. Most strikingly, we show that the FRAP data can be accounted for by the predicted effects of membrane trafficking, even if vesicles do not provide a quantitatively significant flux of Cdc42p to and from the polarization site. Thus vesicle-mediated traffic of Cdc42p is not required to account for the observed Cdc42p dynamics.

RESULTS

Calibrating the reaction-diffusion model

We began by asking whether the reaction-diffusion model, whose parameters were estimated largely based on in vitro biochemical measurements (Goryachev and Pokhilko, 2008; Howell *et al.*, 2009), could reproduce the in vivo GFP-Cdc42p FRAP data from polarized cells treated with latrunculin A (Slaughter *et al.*, 2009). Latrunculin A eliminates polarized vesicle delivery, as well as all endocytosis (Ayscough *et al.*, 1997), leaving only reaction-diffusion mechanisms to polarize Cdc42p.

To simulate a GFP-Cdc42p FRAP experiment, we converted all of the membrane-bound Cdc42p in the steady-state peak (and 1% of the cytoplasmic Cdc42p, as some bleaching is unavoidable) to a "dark" form that participates in all reactions and diffusion but is no longer counted in plotting "visible" unbleached Cdc42p concentration (see *Materials and Methods* for details). The results are shown in kymograph form in Figure 2A and plotted in Figure 2B alongside the experimental data from Slaughter *et al.* (2009; the gray area indicates the mean ± SD of FRAP kinetics in cells). It is evident from this comparison that Cdc42p dynamics are considerably faster in experiments than they are in the model.

To assess which processes might account for the discrepancy between model and experiment, we performed simulations on a one-dimensional membrane in which the separate reactions color-coded in Figure 1A were individually accelerated. To maintain the steady-state conditions as consistently as possible, we multiplied forward and reverse rate constants for each reaction by the same factor and assessed the effect on FRAP kinetics. The results are summarized in Figure 2C and show that changing either the GEF/GAP reactions, the Bem1p complex–membrane interaction, or the Bem1p complex–GTP-Cdc42p association–dissociation reactions had minimal effects on the simulated FRAP. In contrast, accelerating the GDI-mediated reactions progressively speeded the simulated recovery after photobleaching. Thus the GDI rate constants are limiting for Cdc42p dynamics in the model. Similar (though quantitatively

slightly different) results were obtained by accelerating the GDI reactions in simulations on a two-dimensional membrane (Figure 2D).

Increasing the GDI reaction rates in the model had the side effect of elevating the peak concentration of Cdc42p at steady state (Figure 2E). To partially offset this increase, we also doubled the GAP activity, which yielded a sharper steady-state peak of Cdc42p (Figure 2, F and G) that more closely resembled the Cdc42p distribution in vivo (Layton *et al.*, 2011), and reproduced the in vivo FRAP dynamics (Figure 2H). Thus the model is capable of producing a steady state that mimics the shape and dynamics of the Cdc42p peak in yeast cells, if we assume that GDI reaction rates are significantly faster than those estimated from in vitro data.

Our exploration of reaction rate parameters was performed in the context of the membrane diffusion constant used in previous iterations of the model (Goryachev and Pokhilko, 2008; Howell *et al.*, 2009), $D_m = 0.0025\ \mu m^2/s$, which was based on measurements for several proteins in the yeast plasma membrane (Valdez-Taubas and Pelham, 2003). However, another study suggested that diffusion of Cdc42p might be significantly faster, with $D_m = 0.036\ \mu m^2/s$ (Marco *et al.*, 2007). Reasoning that more rapid diffusion might yield faster FRAP dynamics without need for increased GDI reaction rates, we repeated the analysis above using the faster diffusion constant.

With all other parameters as in Howell *et al.* (2009), faster diffusion produced a much shallower and broader Cdc42p peak (Figure 2I). Because a much larger area is bleached to simulate FRAP of the broad peak, the same rate of GDI-mediated Cdc42p delivery over the expanded area causes a significantly larger overall Cdc42p flux, speeding the recovery kinetics (Figure 2J). However, this does not accurately represent FRAP experiments in yeast, in which a smaller peak is subjected to bleaching over a smaller area. To narrow the in silico peak, it was necessary to accelerate reaction rates >30-fold to combat the faster diffusion (Figure 2I and Supplemental Figure S1). With these parameters, the simulated FRAP was much faster than that observed in yeast (Figure 2J).

These simulations illustrate the antagonistic effects of diffusion (which tends to broaden the peak) and recycling (which tends to narrow the peak) on peak shape. For a realistic peak shape, diffusion at $D_m = 0.036\ \mu m^2/s$ requires such rapid recycling that the simulations yield unrealistically fast FRAP. Interestingly, a similar analysis of the vesicle-trafficking model concluded that realistic vesicle-trafficking parameters could yield a polarized Cdc42p distribution if $D_m = 0.0025\ \mu m^2/s$, but not if $D_m = 0.036\ \mu m^2/s$ (Layton *et al.*, 2011). Thus neither this reaction-diffusion model nor the vesicle-trafficking model is capable of generating a realistic Cdc42p peak with the measured dynamics in the face of such rapid diffusion. It is possible that both models are missing fundamental aspects of how Cdc42p polarization takes place. However, the simpler possibility is that in a polarized yeast cell, the actual diffusion constant is closer to $D_m = 0.0025\ \mu m^2/s$, and for the remainder of this report we assume that to be the case.

With $D_m = 0.0025\ \mu m^2/s$, it was necessary to elevate GDI reaction rates 10-fold to obtain realistic FRAP kinetics (see above). The original GDI rate constants in the model were estimated based on in vitro assays using real-time fluorescence resonance energy transfer to monitor the kinetics of interactions (Nomanbhoy *et al.*, 1999). These assays reflect state-of-the-art biochemistry, but there are several possible reasons why they might not accurately reflect the situation in yeast cells. First, the assays used fluorescently tagged recombinant human Cdc42p and GDI proteins, and it could be that the tagging, the recombinant production, or the species of origin make the proteins behave differently. Conversely, the FRAP assays employ GFP-tagged Cdc42p, and it is possible that the GFP tag alters Cdc42p dynamics (e.g., it may bind less tightly to GDI). Second, the in vitro assays used bulk membranes isolated from insect cells, which have a different lipid and protein composition than the internal leaflet of the yeast plasma membrane. Third, the FRAP data in latrunculin-treated cells reflect the sum of all actin-independent Cdc42p recycling mechanisms and not just the GDI-mediated fluxes. Thus some of the flux is probably due to uncharacterized residual pathways, although this component seems to be quantitatively minor (Slaughter *et al.*, 2009). Fourth, yeast cells may contain additional regulatory mechanisms that accelerate GDI-mediated Cdc42p flux (see *Discussion*).

Updating the vesicle-trafficking model

The vesicle-trafficking model developed by Layton *et al.* used a polarization "window," defined as a circle in the center of the simulated plasma membrane, covering 1% of the total membrane area (Layton *et al.*, 2011). However, in preliminary tests, we found that combining that model with the reaction-diffusion system described above led to displacement of the Cdc42p peak away from the trafficking window (unpublished data). This resulted in the direction of vesicle traffic to a site away from the Cdc42p peak, which is unrealistic, as it is in fact GTP-Cdc42p that orients actin cables to direct vesicle traffic (Pruyne *et al.*, 2004). Thus we changed the definition of the window to be the 1% of the membrane area harboring the highest concentration of GTP-Cdc42p. In this way, vesicles are always directed toward the Cdc42p peak, as is thought to occur in vivo. We further modified the Layton model to incorporate endocytic patch movement in response to membrane addition/removal: patches move away from neighboring exocytotic events and toward neighboring endocytotic events (see *Materials and Methods*).

To combine the two models, we need to specify what happens to each molecular species when an endocytic vesicle pinches off the plasma membrane. For cytoplasmic species (Bem1p complex, GDI), we assume that molecules that happened to be in the endocytic patch at the time of vesicle budding are released into the cytoplasm. For Cdc42p, we considered several potential scenarios.

Combined model in which Cdc42p is concentrated into vesicles

As mentioned in the *Introduction*, the ability of vesicle-mediated Cdc42p traffic to generate a polarized Cdc42p distribution depends on whether or not Cdc42p is actively concentrated into vesicles. We first consider a scenario in which both exocytic and endocytic vesicles concentrate Cdc42p according to the rules previously modeled for v-SNARES (Layton *et al.*, 2011). We assume that while a clathrin patch is sitting at the membrane, Cdc42p diffuses into the patch but is then trapped and cannot diffuse back out. That is, the patch acts as a diffusion sink that concentrates Cdc42p, and when the endocytic vesicle buds off, it transports the concentrated Cdc42p to the internal compartment. At the internal compartment, we assume that a 10-fold concentration of Cdc42p into secretory vesicles takes place. This assumption is based on electron microscopy observations indicating that cargo proteins can be concentrated up to 10-fold during vesicle biogenesis (Balch *et al.*, 1994).

We also need to specify what happens to the internalized Cdc42p in terms of its GTP/GDP status. Here we consider two potential scenarios. In the first (hereafter referred to as "frozen" to indicate the unchanging nucleotide state), we assume that any GTP-Cdc42p internalized from the plasma membrane remains GTP-bound, and any GDP-Cdc42p remains GDP-bound. At the internal compartment, both forms retain their starting state and are exported back to the plasma membrane in the same form.

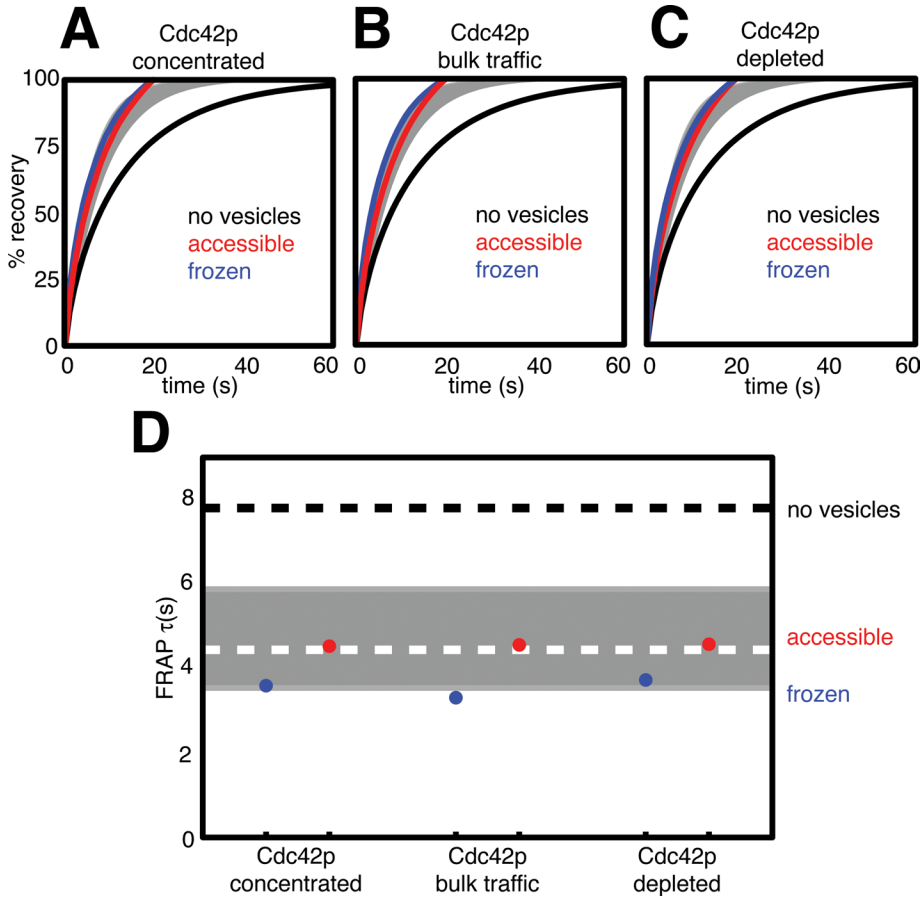

FIGURE 3: Comparison of simulated and experimental FRAP in wild-type cells. Simulated FRAP experiments were conducted for each of the Cdc42p-trafficking scenarios. Blue and red lines show averaged data from 10 simulations each. Black line shows the simulated FRAP with no vesicle traffic from Figure 2H. Gray zone indicates range of experimental data. (A) FRAP assuming that Cdc42p is concentrated into both exocytic and endocytic vesicles. (B) FRAP assuming that Cdc42p undergoes bulk traffic. (C) FRAP assuming that Cdc42p is depleted from endocytic vesicles. (D) Time to 50% simulated FRAP recovery (τ) for all of the simulations. The gray bar indicates the mean (dashed white line) ± SD of experimentally determined τ values in wild-type cells (Slaughter *et al.*, 2009). Black dashed line shows simulated FRAP τ with no vesicle traffic.

Given the significant periods involved in vesicle recycling through internal compartments, the frozen scenario may well be unrealistic. It seems more likely that GTP-bound Cdc42p would hydrolyze the GTP before being shipped back to the plasma membrane. Moreover, any GDP-Cdc42p would be exposed to the cytoplasm, and hence to GDI. Thus, in the second scenario (hereafter referred to as "accessible" to indicate that internalized Cdc42p is subject to GAP and GDI action), we assume that the internalized Cdc42p becomes GDP-bound by the time it reaches the internal compartment, and can then interact with cytoplasmic GDI with the same affinity as cortical Cdc42p.

Starting from the polarized steady state of the parameter-adjusted reaction-diffusion model (Figure 2, F and G), we added vesicle traffic according to these two scenarios. The Cdc42p distributions quickly reached new quasi–steady-state polarized distributions, and we simulated FRAP experiments starting from the Cdc42p distribution attained after allowing the simulation to run for 1 h. Because of stochastic vesicle traffic, each simulation is a little different from the next, so we simulated 10 FRAP experiments for each scenario and calculated an average recovery curve. The addition of vesicle traffic to the reaction-diffusion model speeded FRAP kinetics (Figure 3A). Simulations assuming that internalized Cdc42p was frozen (Figure 3A, blue, $\tau \approx 6$ 3.6 s) displayed slightly faster recovery kinetics than simulations assuming that internalized Cdc42p was accessible (Figure 3A, red, $\tau \approx 4.5$ s). For comparison, the experimentally observed behavior (mean ± SD) is displayed in gray. There is a good match between simulated and observed FRAP behavior.

Combined model in which Cdc42p is not concentrated into vesicles

We next consider a scenario in which there is no concentration of Cdc42p into vesicles. Previous results suggested that such "bulk" traffic would act to disperse Cdc42p, rather than to reinforce Cdc42p polarization (Layton *et al.*, 2011). We assume that while a clathrin patch is sitting at the membrane, Cdc42p diffuses in and out of the patch unhindered. When the endocytic vesicle internalizes, it transports whatever Cdc42p is present to the internal compartment. Similarly, vesicles budding from the internal compartment carry whatever Cdc42p concentration was present at the time of vesicle budding from the membrane. As with the model described above, we consider scenarios in which the nucleotide bound to internalized Cdc42p is either frozen or accessible to GAPs/GDI.

The results from these simulations are shown in Figure 3B. Remarkably, bulk traffic led to almost identical effects as the concentrated Cdc42p traffic considered above (indeed, the frozen scenario predicted even faster kinetics, with $\tau \approx 3.3$ s).

We also tested a more extreme scenario, in which Cdc42p is depleted from endocytic vesicles. Here we assume that while a clathrin patch is sitting at the membrane, Cdc42p diffuses out of the patch but cannot diffuse back in. That is, the patch acts as an "anti-sink" that excludes Cdc42p. When the endocytic vesicle internalizes, it transports any residual Cdc42p to the internal compartment. Vesicles budding from the internal compartment carry the Cdc42p present at the time of vesicle budding. The results from these simulations are shown in Figure 3C. Astonishingly, the simulated FRAP curves were almost indistinguishable from those of the model in which Cdc42p was actively concentrated into vesicles (Figure 3A).

The results from all six scenarios considered above are summarized in Figure 3D. All vesicle-containing models accelerated FRAP recovery compared with the reaction-diffusion model, and models in which the internalized Cdc42p was accessible all produced an equally good match to the experimentally observed FRAP in wild-type cells (gray bar).

Membrane traffic (rather than Cdc42p flux) accounts for the faster FRAP kinetics

To ask how Cdc42p fluxes varied in each of the models, we first examined the concentration of Cdc42p in the internal compartment from which the vesicle-mediated flux originates (Figure 4A). In the

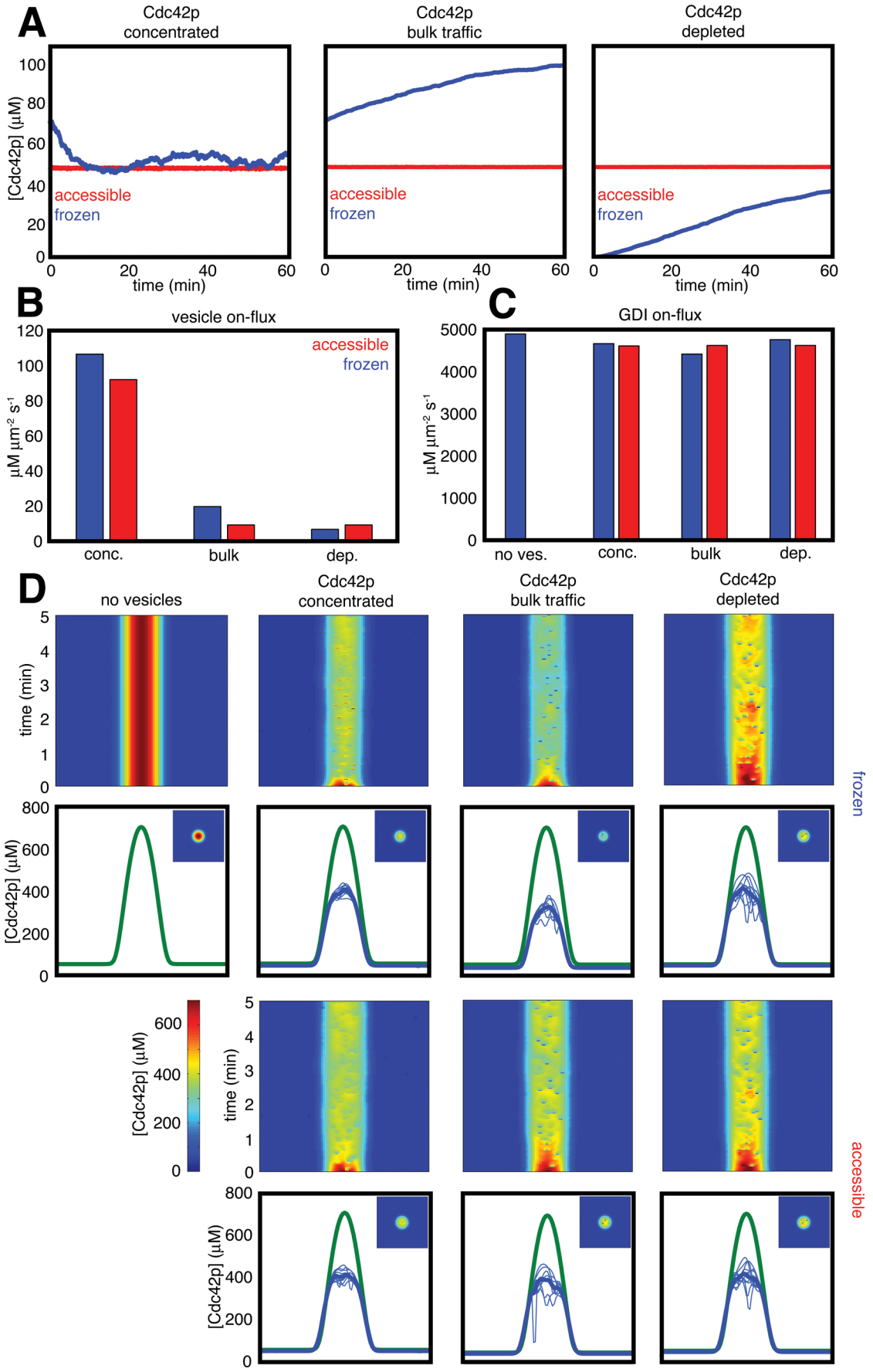

FIGURE 4: Effect of simulated vesicle traffic on the steady-state Cdc42p distribution. (A) Concentration of Cdc42p in the internal compartment. Simulations were initiated with the plasma membrane Cdc42p distribution provided by the

three models that assumed that Cdc42p was accessible to cytoplasmic GDI, the GDI acted as a buffer that maintained a steady Cdc42p concentration in the internal compartment. In contrast, when Cdc42p was frozen, the models behaved differently. The model assuming that Cdc42p is actively concentrated into both endocytic and exocytic vesicles developed a fluctuating concentration that was similar to that in the accessible (GDI-buffered) models. Unexpectedly, however, the bulk traffic model and the model in which Cdc42p is depleted from endocytic vesicles both accumulated Cdc42p in the internal compartment over the course of the simulation (Figure 4A). Because endocytosis occurs more frequently within the window than elsewhere, and Cdc42p is highly concentrated in the window by the reaction-diffusion system, endocytosis in polarized cells would deliver far more concentrated Cdc42p to the internal compartment than it would in nonpolarized cells. Thus, in both models, the Cdc42p in that compartment builds up until a new steady state is reached. Although the model that concentrates Cdc42p into vesicles delivers even more Cdc42p to the internal compartment, the Cdc42p is then concentrated 10-fold into the vesicles departing to the plasma membrane, so the steady-state concentration of Cdc42p remains lower than in the bulk-traffic model.

We then calculated the average vesicle-mediated fluxes from the internal compartment to the plasma membrane that was bleached by simulated FRAP (Figure 4B). As expected, the fluxes differed markedly, being lowest for the model assuming that Cdc42p is depleted from and highest for the model assuming that Cdc42p is concentrated into vesicles.

If the vesicle-mediated Cdc42p fluxes differ by over 15-fold, how is it that all of the models yield comparable predictions regarding FRAP dynamics? The GDI-mediated Cdc42p flux to the bleached region from the cytoplasm was over 40-fold higher than even the highest vesicle-mediated flux (Figure 4C). Thus the GDI-mediated flux dominates FRAP recovery dynamics, and vesicle-mediated Cdc42p fluxes are minor by comparison.

If vesicle-mediated Cdc42p flux does not contribute significantly to FRAP dynamics, then why does adding vesicle traffic speed FRAP recovery? The GDI-mediated Cdc42p flux is not significantly different in the presence or absence of vesicles (indeed, it is slightly smaller in the presence of vesicles; Figure 4C). Thus the answer must lie with the vesicle-mediated flux of membrane, rather than the flux of Cdc42p itself.

Membrane traffic lowers the polarized Cdc42p concentration

How does membrane traffic speed FRAP recovery? Examination of the effect of vesicle traffic on the polarized Cdc42p distribution revealed that, for all trafficking scenarios, vesicle traffic lowered the peak Cdc42p concentration relative to the model with only the reaction-diffusion system (Figure 4D). This effect was most severe for the bulk-traffic model, in which Cdc42p was then frozen, presumably because that model accumulated a larger pool of Cdc42p in the internal compartment (thereby depleting it from the plasma membrane; Figure 4A). Consistent with that observation, this model also exhibited the speediest FRAP recovery kinetics (Figure 3).

The finding that vesicle traffic reduced the amount of Cdc42p at the polarization site provides an explanation for the faster kinetics of FRAP recovery. The time taken for a constant flux of unbleached Cdc42p to replenish a polarized pool of Cdc42p will depend on the size of that pool, with a smaller pool filling faster than a larger one. As FRAP curves are normalized to the final recovered fluorescence level, this feature can account for our observations.

Why does membrane traffic reduce the amount of Cdc42p at the polarization site? For the models in which Cdc42p is not concentrated into vesicles, this is in fact the predicted outcome (Layton *et al.*, 2011), as fusion of secretory vesicles would dilute the polarized Cdc42p, whereas endocytosis would remove concentrated Cdc42p; both contribute to reducing the peak concentration. However, when Cdc42p is concentrated into forming vesicles, vesicle traffic was previously shown to develop a polarized distribution in the absence of any reaction-diffusion system (Layton *et al.*, 2011), so we were initially surprised that it would have a similarly perturbing effect. Although the total Cdc42p concentration on secretory vesicles in this model is much higher, it is still less than the peak Cdc42p concentration in the reaction-diffusion model. In addition, vesicles deliver much less GTP-Cdc42p to the polarization site than the level sustained by the reaction-diffusion mechanism, and the vesicles do not carry the Bem1p complex. Thus vesicle fusion dilutes GTP-Cdc42p and Bem1p, while endocytosis removes these proteins from the peak, lowering overall Cdc42p concentration.

We note that the polarity-perturbing effect of vesicle traffic in our combined model is consistent with a previous study that posited the existence of an actin-dependent, negative-feedback loop (Ozbudak *et al.*, 2005). In that study, the feedback loop was thought to be responsible for generating movement of the polarity site, and our stochastic vesicle traffic simulations suggest that vesicle traffic may indeed have that effect. However, the physiological relevance of polarity site movement to normal prebudding polarity in yeast remains unclear (Howell *et al.*, 2012).

Effect of an increased rate of vesicle trafficking, as found in other fungi

The analysis presented thus far indicates that the vesicle-mediated Cdc42p flux does not contribute significantly to FRAP dynamics in yeast, and that this is because even the most concentrated vesicular Cdc42p flux we simulated is tiny when compared with the GDI-mediated Cdc42p flux. The vesicle-mediated flux of Cdc42p reflects the product of the Cdc42p concentration on the vesicles and the rate of vesicle traffic. Thus a major limiting factor for Cdc42p flux is the relatively slow rate of vesicle traffic in yeast.

reaction-diffusion system in the absence of vesicle traffic (as in Figure 2F). Cdc42p in the internal compartment was initially the steady-state amount in nonpolarized cells. Graphs illustrate the evolution of the internal compartment Cdc42p concentration with time for the indicated trafficking scenarios. (B) The average Cdc42p flux mediated by vesicle traffic from the internal compartment to the polarization site as calculated from the simulations in (A). (C) The average Cdc42p flux mediated by the GDI from the cytoplasm to the polarization site as calculated from the simulations in (A). (D) Effect of different Cdc42p trafficking scenarios on Cdc42p polarization. Kymographs of a central slice through the plasma membrane (*x*-axis) show effect of vesicle traffic in the first 5 min (time: *y*-axis). Note that individual vesicle fusion events appear red when vesicles carry concentrated Cdc42p, but blue when they do not. For comparison, the simulated Cdc42p steady state of the reaction-diffusion model is also shown ("no vesicles"). Graphs indicate averaged Cdc42p profiles (dark blue) calculated from 10 different time points (light blue) of the simulations in (A), compared with the reaction-diffusion model (green). Insets, snapshots of the Cdc42p distributions at 60 min show two-dimensional profiles.

Compared with yeasts, related filamentous fungi that use similar polarity mechanisms are capable of much faster polar growth, which is thought to involve a higher trafficking rate for both secretory and endocytic vesicles. Thus, in these systems, the vesicular Cdc42p flux might be comparable to the GDI-mediated flux. To model this situation, we accelerated exocytic and endocytic rates.

Assuming bulk traffic of Cdc42p or depletion of Cdc42p from the endocytic vesicles, faster traffic reduced the peak Cdc42p concentration and broadened the peak (Figure 5). At 32-fold-faster traffic, the remaining "peak" covered over half of the plasma membrane. Similar results were obtained whether or not internal Cdc42p pools were accessible to GAP and GDI activity (Figure 5). Thus fast vesicle traffic that does not concentrate polarity regulators would drastically reduce polarization.

If Cdc42p was concentrated into both exocytic and endocytic vesicles, the models were slightly better at maintaining a polarized Cdc42p profile in the face of faster traffic (Figure 5). Even in these cases, polarity was significantly reduced at 32-fold-faster traffic. Examination of kymographs (Figure 5A) indicates that as the peak broadens with faster vesicle traffic, the concentrated Cdc42p delivered by vesicles is also spread over a larger area. This feature depends on exactly how the target sites of vesicle fusion are picked. In our model, we specified stochastic delivery to the sites containing the highest instantaneous GTP-Cdc42p concentration, but in real cells vesicles are delivered to the plasma membrane by actin cables. Cable position may be less sensitive to fluctuations in the GTP-Cdc42p distribution than is the vesicle delivery in our model, potentially enabling cells to retain a more focused polarization site. Thus, fast, active trafficking of Cdc42p has the potential to counteract the polarity-perturbing effect of fast membrane traffic, at least in principle.

DISCUSSION

We present a mathematical model that combines two processes thought to contribute to polarity establishment and maintenance in *S. cerevisiae*: a reaction-diffusion system with positive feedback via the Cdc42p-directed GEF, and vesicle traffic targeted by GTP-Cdc42p.

Comparison of simulated and experimental Cdc42p FRAP in cells lacking F-actin

A model of the reaction-diffusion system had been developed previously, with parameter estimates based on experimental data (Goryachev and Pokhilko, 2008; Howell *et al.*, 2009). However, with those parameters, we found that simulated Cdc42p dynamics were much slower than those measured in vivo by FRAP in latrunculin-treated cells, which lack targeted vesicle traffic (Slaughter *et al.*, 2009). Our simulations indicated that the key parameters limiting Cdc42p dynamics in the model involve GDI-mediated interactions. Increasing the GDI rate constants 10-fold made the simulated FRAP kinetics comparable to those measured experimentally. The model GDI rate constants were estimated based on state-of-the-art biochemical assays (Nomanbhoy *et al.*, 1999), but it remains possible (as discussed in *Results*) that technical issues, such as fluorescent tags or lipid composition, might account for the apparent discrepancies between the in vitro and in vivo data. Alternatively, it could be that yeast cells contain additional regulatory mechanisms that can speed GDI-mediated Cdc42p flux. In mammalian cells, GDI phosphorylation and interactions with signaling proteins have been reported to promote the release of the GTPase from the GDI (Garcia-Mata *et al.*, 2011). Our findings may indicate that similar (currently uncharacterized) mechanisms apply in yeast.

We also simulated the effects of the more rapid diffusion constant estimated by an experimental study using FRAP of nonpolarized, latrunculin-treated cells induced to overexpress a GTP-locked version of Cdc42p (Marco *et al.*, 2007). As expected, faster diffusion led to spreading of the Cdc42p peak, making it much shallower and broader. This could be counteracted by greatly accelerating the recycling reactions, but that compensatory change led to simulated FRAP kinetics much faster than those measured in vivo. Thus, with fast diffusion, neither the current reaction-diffusion model nor the vesicle-trafficking model (Layton *et al.*, 2011) could recapitulate the observed Cdc42p distribution and dynamics in yeast. The simplest possibility to account for this is that diffusion is not as rapid as estimated by Marco *et al.* (2007). Interestingly, time-lapse imaging of polarity establishment indicated that the polarity peak (as visualized using Bem1p-GFP) is initially quite broad, and then condenses to a narrower and sharper distribution (Howell *et al.*, 2009). It may be that initial polarization occurs in a rapid-diffusion context, creating a broad peak that then induces local changes that slow diffusion in its vicinity.

To enable subsequent comparison of models containing vesicle traffic with in vivo FRAP measurements on wild-type cells, we retained the original (slower) diffusion constant but adjusted the GDI reaction parameters so that model simulations matched the experimental observations in cells lacking F-actin.

Vesicle-mediated membrane flux speeds FRAP recovery regardless of whether or not the vesicles carry Cdc42p

An influential hypothesis about polarity establishment in yeast posits that delivery of Cdc42p on secretory vesicles, which are preferentially targeted to Cdc42p-rich sites at the plasma membrane, constitutes a self-reinforcing, positive-feedback loop (Wedlich-Soldner *et al.*, 2003). However, reinforcement would only occur if the concentration of Cdc42p and other polarity factors on the exocytic vesicles were high enough to elevate their concentration at the target membrane; otherwise, vesicle fusion would dilute the local factors, reducing polarity (Layton *et al.*, 2011). Thus the validity of the hypothesis critically depends on whether vesicles carry sufficiently concentrated Cdc42p.

As secretory vesicles fuse with the plasma membrane shortly after they are produced, wild-type yeast cells contain very few vesicles, making it difficult to assess how much Cdc42p they might carry. That they do carry some Cdc42p has been inferred from fractionation analyses of *sec* temperature-sensitive mutants (Wedlich-Soldner *et al.*, 2003; Orlando *et al.*, 2011), which accumulate large numbers of secretory vesicles at restrictive temperature. However, these backed-up vesicles might become populated with Cdc42p after they form (perhaps via GDI-mediated delivery from the cytoplasm), in which case the amount of Cdc42p that they carry might not accurately reflect the amount present on short-lived, wild-type vesicles. Thus the question of how much Cdc42p is normally carried by vesicles remains experimentally intractable.

The observation that the kinetics of Cdc42p FRAP recovery were faster in wild-type cells (which contain both a reaction-diffusion system and directed vesicle traffic) than in latrunculin-treated cells (containing only the reaction-diffusion system) has been taken as evidence that vesicle-mediated Cdc42p traffic provides a significant Cdc42p flux, consistent with the idea that such traffic would reinforce polarity (Slaughter *et al.*, 2009). However, our simulations indicate that vesicle-mediated membrane traffic would speed Cdc42p FRAP recovery even if the vesicles did not carry significant amounts of Cdc42p. Membrane traffic reduced the amount of Cdc42p at the

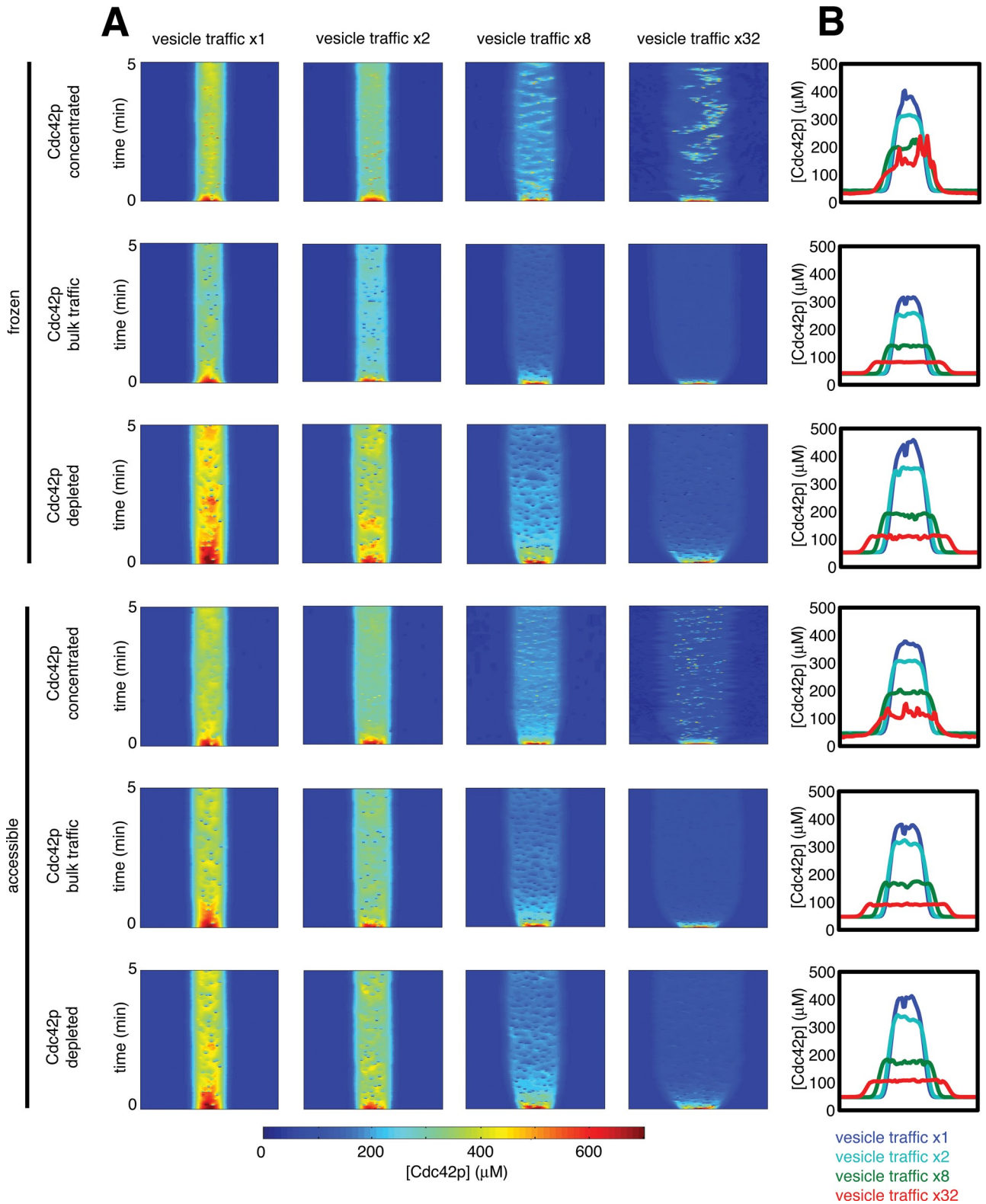

FIGURE 5: Effect of increasing the vesicle-trafficking rate. (A) Kymographs displayed as in Figure 4D. Simulations were conducted with yeast-rate traffic or faster traffic (2×, 8×, or 32×). (B) Averaged Cdc42p distributions. Ten snapshots were averaged to derive each profile.

polarization site, so that an equivalent Cdc42p flux (mediated by the GDI) took less time to replenish the Cdc42p. The faster FRAP dynamics were simply due the reduced Cdc42p level at the polarization site, and not due to vesicle-mediated Cdc42p flux.

Our models produced a good match for the FRAP data in untreated cells, with no further parameter adjustments beyond those discussed in the section *Calibrating the reaction-diffusion model* for the reaction-diffusion system. As with the previous analysis

(Slaughter *et al.*, 2009), we assumed that the reaction-diffusion system is identical in latrunculin-treated and untreated cells. Because latrunculin treatment triggers stress-response pathways (Harrison *et al.*, 2001), we cannot rule out the possibility that such stress alters GDI parameters in unknown ways. Nevertheless, our findings indicate that the observed differences between latrunculin-treated and untreated cells can in principle be fully accounted for by effects of membrane traffic.

We compared models in which Cdc42p was concentrated onto vesicle membranes, depleted from vesicles, or neither concentrated nor depleted (bulk traffic). Remarkably, the degree to which Cdc42p became concentrated into vesicles made almost no difference to the simulated FRAP. This was because vesicles delivered a quantitatively minor Cdc42p flux compared with the large GDI-mediated flux, even assuming that Cdc42p is concentrated ~10-fold during vesicle biogenesis. The main reason for this is that the rate of vesicle delivery to the plasma membrane in yeast is relatively slow, limiting the amount of Cdc42p that can realistically be delivered.

Faster vesicle trafficking would disrupt polarity, suggesting a need for compensatory mechanisms to maintain polarity

As a fundamental parameter limiting vesicular Cdc42p flux is the rate of vesicle traffic, we considered the consequences of increasing the rate of such traffic. With 32-fold faster traffic, membrane traffic that did not carry concentrated Cdc42p effectively destroyed the peak. Thus rapid membrane traffic dissipates polarity to a degree that can no longer be counteracted by the reaction-diffusion system.

Filamentous fungi are related to yeasts but can sustain much faster rates of vesicle trafficking at the hyphal tips. In such fungi, the hyphal tip membrane is completely renewed every few seconds, so there must be an effective way to recycle polarity regulators that are displaced from the tip by vesicle delivery. Our simulations suggest that the yeast reaction-diffusion recycling mechanism, although sufficient to withstand yeast-rate vesicle traffic, would be ineffective at maintaining polarity in fast-growing fungal hyphae. Thus either filamentous fungi have a reaction-diffusion system better able to rapidly recycle polarity factors or they may possess parallel pathways to recycle such factors.

On the basis of the observation that endocytosis is important for polarity maintenance in *Aspergillus nidulans* (Upadhyay and Shaw, 2008), Shaw and colleagues proposed that polarity factors are recycled to the hyphal tip by endocytosis from the lateral membranes and redelivery to hyphal tips by exocytosis (Shaw *et al.*, 2011). Consistent with that idea, our simulations assuming that Cdc42p is heavily concentrated into vesicles were better able to maintain some degree of polarity. This raises the question of whether Cdc42p is indeed concentrated into such vesicles.

The filamentous fungus *Ashbya gossypii* is a close relative of *S. cerevisiae* (Dietrich *et al.*, 2004), and uses a similar molecular machinery for polarization (Schmitz and Philippsen, 2011). In fast-growing *A. gossypii* hyphae, a spitzenkörper containing a dense cluster of secretory and endocytic vesicles forms near the apical tip. This cluster provides a convenient tool to explore whether polarity regulators are concentrated on such vesicles. Although several vesicle-associated proteins were localized to the spitzenkörper as well as to the hyphal tip, Cdc42p (like Bem1p and the GEF Cdc24p) was concentrated at the tip but not in the spitzenkörper (Kohli *et al.*, 2008). Similarly, a recent study on *Neurospora crassa* found that Cdc42p was concentrated at the hyphal tip but not the spitzenkörper (Araujo-Palomares *et al.*, 2011). Thus in these fungi it seems unlikely that Cdc42p is present at high concentration on secretory and endocytic vesicles.

In summary, a yeast-like reaction-diffusion system would be unable to effectively withstand the deluge of vesicles delivered to the front in fast-growing hyphae. A potential compensatory mechanism would exploit the high rate of vesicle traffic in hyphae to deliver and recycle polarity factors, but the available evidence does not support the idea that Cdc42p itself is recycled in this manner, and it will be interesting to determine whether such a regulator exists.

Conclusions

Mathematical modeling of polarity establishment and maintenance in yeast reveals a potential dilemma for cells that grow by polarized vesicle traffic. A reaction-diffusion system with positive feedback can effectively establish a specialized front with concentrated polarity factors. Those factors then orient the actin cytoskeleton to initiate polarized vesicle delivery to the front. However, because the vesicles do not appear to carry comparably concentrated polarity factors, vesicle fusion at the front dilutes the polarity regulators. The net effect is a reduced local polarity factor concentration, whose fluctuating level reflects an ongoing battle between the reaction-diffusion system (which recruits more factors) and vesicle delivery (which adds more membrane). For budding yeast, our results suggest that the reduced Cdc42p concentration resulting from vesicle traffic suffices to account for the observed difference in FRAP dynamics between cells that do or do not contain polymerized actin.

MATERIALS AND METHODS

Assumptions and equations of the reaction-diffusion model

The Goryachev model (Goryachev and Pokhilko, 2008; Howell *et al.*, 2009) calculates how the concentrations of eight molecular species vary in space and time as a result of reactions and diffusion. The species are as follows (all species are on the plasma membrane unless otherwise stated):

GTP-Cdc42p (Cdc42T), GDP-Cdc42p (Cdc24D), Bem1p complex (BemGEF, or BemGEFc when cytoplasmic), Bem1p complex bound to GTP-Cdc42p (BemGEF42), cytoplasmic GDI (GDIc), and GDI bound to GDP-Cdc42p (GDI42, or GDI42c when cytoplasmic).

The equations governing the behavior of these species are as follows:

$$\frac{\partial}{\partial t}\mathrm{Cdc42T} = \left(k_{2a}\mathrm{BemGEF} + k_{3}\mathrm{BemGEF42}\right)\cdot\mathrm{Cdc42D} - k_{2b}\mathrm{Cdc42T} - k_{4a}\mathrm{BemGEF}\cdot\mathrm{Cdc42T} + k_{4b}\mathrm{BemGEF42} - k_{7}\mathrm{BemGEFc}\cdot\mathrm{Cdc42T} + \mathrm{D_m}\Delta\mathrm{Cdc42T}$$

$$\frac{\partial}{\partial t}\mathrm{BemGEF42} = k_{4a}\mathrm{BemGEF}\cdot\mathrm{Cdc42T} - k_{4b}\mathrm{BemGEF42} + k_{7}\mathrm{BemGEFc}\cdot\mathrm{Cdc42T} + \mathrm{D_m}\Delta\mathrm{BemGEF42}$$

$$\frac{\partial}{\partial t}\mathrm{BemGEF} = k_{1a}\mathrm{BemGEFc} - k_{1b}\mathrm{BemGEF} - k_{4a}\mathrm{BemGEF}\cdot\mathrm{Cdc42T} + k_{4b}\mathrm{BemGEF42} + \mathrm{D_m}\Delta\mathrm{BemGEF}$$

$$\frac{\partial}{\partial t}\mathrm{BemGEFc} = \eta\left[k_{1b}\mathrm{BemGEF} - \left(k_{1a} + k_{7}\mathrm{Cdc42T}\right)\cdot\mathrm{BemGEFc}\right] + \mathrm{D_c}\Delta\mathrm{BemGEFc}$$

$$\frac{\partial}{\partial t}\mathrm{Cdc42D} = k_{2b}\mathrm{Cdc42T} - \left(k_{2a}\mathrm{BemGEF} + k_{3}\mathrm{BemGEF42}\right)\cdot\mathrm{Cdc42D} + k_{6b}\mathrm{GDI42} - k_{6a}\mathrm{GDIc}\cdot\mathrm{Cdc42D} + \mathrm{D_m}\Delta\mathrm{Cdc42D}$$

$$\frac{\partial}{\partial t}\mathrm{GDI42} = k_{6a}\mathrm{GDIc}\cdot\mathrm{Cdc42D} - k_{6b}\mathrm{GDI42} + k_{5a}\mathrm{GDI42c} - k_{5b}\mathrm{GDI42} + \mathrm{D_m}\Delta\mathrm{GDI42}$$

$$\frac{\partial}{\partial t}\mathrm{GDI42c} = \eta\left(k_{5b}\mathrm{GDI42} - k_{5a}\mathrm{GDI42c}\right) + \mathrm{D_c}\Delta\mathrm{GDI42c}$$

$$\frac{\partial}{\partial t}\mathrm{GDIc} = \eta\left(k_{6b}\mathrm{GDI42} - k_{6a}\mathrm{GDIc}\cdot\mathrm{Cdc42D}\right) + \mathrm{D_c}\Delta\mathrm{GDIc}$$

The assumptions of this model, parameterized as in Howell *et al.* (2009; see Table 1), include the following:

1. Diffusion of all membrane-bound species occurs with the same diffusion constant. We assumed $D_m = 0.0025$ μm^2/s (Valdez-Taubas and Pelham, 2003; Goryachev and Pokhilko, 2008) for most simulations, and $D_m = 0.036$ μm^2/s (Marco *et al.*, 2007), where noted.
2. Diffusion of all cytoplasmic species is so fast that the cytoplasm is effectively well mixed.
3. Cdc42p GTP hydrolysis is described by a first-order rate constant representing the effect of several Cdc42p-directed GAPs. This assumes that all GTP-Cdc42p molecules are equally accessible to the GAPs regardless of location.
4. Cdc42p GDP/GTP exchange is catalyzed by the Bem1p-GEF complex at the membrane: spontaneous exchange and exchange due to GEF that is not bound to Bem1p are assumed to be negligible. The GTP-Cdc42p–bound Bem1p-GEF is assumed to have twofold higher catalytic activity than the nonbound Bem1p-GEF (Howell *et al.*, 2009).
5. Both cytoplasmic and membrane-bound Bem1p complex can bind to GTP-Cdc42p, but the full complex stays on the membrane. Cdc42p does not undergo GTP hydrolysis while bound to the Bem1p complex. When this complex dissociates, both GTP-Cdc42p and the Bem1p complex are initially on the membrane.
6. Cytoplasmic GDI can bind GDP-Cdc42p, but not GTP-Cdc42p, to generate an initially membrane-bound Cdc42p-GDI complex that can then exchange between membrane and cytoplasm. Cdc42p cannot exchange GDP for GTP while bound to GDI. Membrane-bound Cdc42p-GDI complex can dissociate to yield GDP-Cdc42p on the membrane and GDI in the cytoplasm.
7. The cytoplasmic volume is assumed to be 100 times larger than the membrane "volume." One way to think of this is that the cytoplasm is the volume enclosed by a sphere of 5-μm diameter, while the membrane is the volume of a 10-nm-thick shell at the boundary of the sphere.

Assumptions of the vesicle-trafficking model

The following assumptions correspond to the "uniform-fill" model of Layton (Layton *et al.*, 2011). As with the Goryachev model, the plasma membrane represents the area of the surface of a 5-μm sphere, and species on the membrane diffuse with D_m = 0.0025 μm^2/s.

1. There is an internal compartment, representing the endo-membrane system relevant to Cdc42p recycling, with membrane area equal to 70% of the plasma membrane area. Owing to continuous vesicle fusion and fission, this compartment is assumed to be well mixed (i.e., concentrations of species on this membrane are uniform).
2. Endocytosis is modeled as a two-step process: cargo trapping followed by internalization. First, a patch with 1/10,000th the area of the plasma membrane (equivalent to a 50-nm-diameter vesicle) forms at a specified location (see point 6 below) at the plasma membrane. We model an integral membrane "cargo" protein that traffics like a v-SNARE and does not react with the

Description		Parameter	Howell (2009)	This work	Units
Cdc42D + BemGEF	→*Cdc42T + BemGEF*	k_{2a}	0.16	0.16	μM^{-1} s^{-1}
Cdc42D + BemGEF42	→*Cdc42T + BemGEF42*	k_3	0.35	0.35	μM^{-1} s^{-1}
Cdc42T	→*Cdc42D*	k_{2b}	0.315	0.63	s^{-1}
Cdc42D + GDIc	→*GDI42*	k_{6a}	1.5	15	μM^{-1} s^{-1}
GDI42	→*Cdc42D + GDIc*	k_{6b}	0.5	5	s^{-1}
GDI42	→*GDI42c*	k_{5b}	0.13	1.3	s^{-1}
GDI42c	→*GDI42*	k_{5a}	0.9	9	s^{-1}
Cdc42T + BemGEF	→*BemGEF42*	k_{4a}	10	10	μM^{-1} s^{-1}
Cdc42T + BemGEFc	→*BemGEF42*	k_7	10	10	μM^{-1} s^{-1}
BemGEF42	→*Cdc42T + BemGEF*	k_{4b}	10	10	s^{-1}
BemGEFc	→*BemGEF*	k_{1a}	10	10	s^{-1}
BemGEF	→*BemGEFc*	k_{1b}	10	10	s^{-1}
	Volume ratio	η	0.01	0.01	
	Diffusion constant (membrane)	D_m	0.0025	0.0025	μm^2 s^{-1}
Total [Cdc42p]			5	5	μM
Total [BemGEF]			0.017	0.017	μM
Total [GDI]			5	5	μM

TABLE 1: Parameter values for the reaction-diffusion model.

polarity-relevant proteins of the reaction-diffusion model. This cargo protein represents an aggregate of actively endocytosed species that determines when the patch fills up, and the endocytic patch acts as a diffusion sink that concentrates the cargo. When a specified "fill-level" of cargo is reached, the patch undergoes internalization: the patch area and content (cargo plus any Cdc42p) are transferred to the internal compartment after a 15-s "dead time" representing the process of vesicle invagination and abscission.

3. Exocytosis is modeled as an instantaneous transfer of a patch of membrane with 1/2500th the area of the plasma membrane (equivalent to a 100-nm-diameter vesicle) and content (cargo plus any Cdc42p) from the internal compartment to a specified location (see point 5 below) at the plasma membrane. The cargo concentration in the transferred "vesicle" is 10-fold higher than in the internal compartment.
4. Endocytic patches form at a frequency of 1.67 s^{-1}. Exocytic vesicles, with four times the area, traffic at fourfold lower frequency, so that the total membrane area does not change (apart from stochastic fluctuations).
5. Exocytic vesicles fuse at a random location within the polarization "window," which encompasses 1% of the total plasma membrane area. Because actin cables direct all exocytic traffic toward the polarization site, no exocytosis occurs outside the window.
6. Endocytic patches can form anywhere, but they form with 40-fold higher probability (per unit area) in the window. The higher probability that a patch forms within the window derives from the experimental observation that actin patches are concentrated near the polarization site in polarized unbudded cells.

Combining the reaction-diffusion and vesicle-trafficking models

The new model cell has three compartments: plasma membrane, cytoplasm, and internal compartment (endomembrane system). The plasma membrane is modeled as a square with area equivalent to that of a 5-μm-diameter sphere (78.5 μm^2). The square is subdivided into 100 × 100 grid points, and molecular species diffuse between neighboring points. The left/right and top/bottom edges are diffusionally connected to avoid edge effects. The cytoplasm has volume 100-fold greater than that of the plasma membrane and is considered well mixed, as in the reaction-diffusion model. The internal compartment is 70% as large as the plasma membrane and is considered well mixed, as in the vesicle-trafficking model.

Vesicles traffic between the internal compartment and the plasma membrane, as they do in the Layton model (Layton *et al.*, 2011), except that the window is defined as the 1% of the plasma membrane that has the highest GTP-Cdc42p concentration, rather than a circular zone in the middle of the plasma membrane. This does not explicitly take into account the actin cables that link GTP-Cdc42p (which nucleates actin cable formation) to vesicle traffic (which is directed toward the actin cable termini by myosin V). Because the detailed biochemical parameters governing cable nucleation/growth/detachment and vesicle delivery/fusion are poorly understood, we consider this an acceptable simplification that directly links vesicle traffic to a restricted area containing high GTP-Cdc42p concentration. We note that in principle, the window defined in this manner need not consist of a physically contiguous area. However, in practice, our simulations do exhibit a clear Cdc42p peak toward which vesicles traffic.

In this work, we consider six different trafficking models for Cdc42p (for a list of programs, see Table 2):

1. Cdc42p concentrated into vesicles, GTP/GDP state frozen: Exocytic vesicles carry GTP-Cdc42p and GDP-Cdc42p at 10-fold higher concentration than that of the corresponding species in the internal compartment. Endocytic vesicles also carry more concentrated Cdc42p, because the endocytic patch acts as a diffusion sink for Cdc42p in the same way that it does for v-SNARE cargo. All forms of Cdc42p are concentrated by this process, including GDI-bound GDP-Cdc42p and Bem1p-bound GTP-Cdc42p. However, at the time of internalization, any bound GDI or Bem1p complexes are released into the cytoplasm, while Cdc42p is delivered to the internal compartment.
2. Cdc42p concentrated into vesicles and accessible to GAP/GDI: Cdc42p traffic in this model is similar to that in 1, except that all endocytosed Cdc42p is converted to GDP-Cdc42p at the internal compartment, where it can bind cytoplasmic GDI and exchange with the cytoplasmic pool according to the same rules as plasma membrane GDP-Cdc42p.
3. Cdc42p bulk traffic, GTP/GDP state frozen: Exocytic vesicles carry GTP-Cdc42p and GDP-Cdc42p at the same concentration as that of the corresponding species in the internal compartment. During the cargo-trapping phase of endocytosis, all forms of Cdc42p diffuse in and out of the patch unhindered. At the time of internalization, the Cdc42p present in the patch is delivered to the internal compartment, and any bound GDI or Bem1p complexes are released into the cytoplasm.
4. Cdc42p bulk traffic, accessible to GAP/GDI: Cdc42p traffic in this model is similar to that in 3 except that all endocytosed Cdc42p is converted to GDP-Cdc42p at the internal compartment, where it can bind cytoplasmic GDI and exchange with the cytoplasmic pool according to the same rules as plasma membrane GDP-Cdc42p.
5. Cdc42p depleted from vesicles, GTP/GDP state frozen: Exocytic vesicles carry GTP-Cdc42p and GDP-Cdc42p at the same concentration as that of the corresponding species in the internal compartment. Endocytic vesicles carry less Cdc42p, because the endocytic patch acts as a diffusion "anti-sink" for Cdc42p: during the cargo-trapping phase of endocytosis, all forms of Cdc42p diffuse out of the patch but cannot diffuse in. At the time of internalization, the Cdc42p remaining in the patch is delivered to the internal compartment, and any bound GDI or Bem1p complexes are released into the cytoplasm.
6. Cdc42p depleted from vesicles, accessible to GAP/GDI: Cdc42p traffic in this model is similar to that in 5, except that all endocytosed Cdc42p is converted to GDP-Cdc42p at the internal compartment, where it can bind cytoplasmic GDI and exchange with the cytoplasmic pool according to the same rules as plasma membrane GDP-Cdc42p.

In all models, the Bem1p complex is present only on the plasma membrane or in the cytoplasm, and not in the internal compartment. Thus no GTP loading of Cdc42p occurs at the internal compartment. For the "frozen" models, the same is true for the GAPs and GDI. Thus no GTP hydrolysis by Cdc42p occurs at the internal compartment. But for the "accessible" models, we assume that GAP access causes GTP hydrolysis for all internal Cdc42p and that the GDI can exchange Cdc42p between the cytoplasm and the internal compartment in the same way that it can between the cytoplasm and plasma membrane.

Simulation type	Folder	Description
No vesicle simulations	reaction_diffusion\	Runs the reaction-diffusion model for a while and then bleaches a FRAP circle, diameter determined automatically, and 1% of the cytoplasm.
Vesicle simulations	reaction_diffusion_vesicle\ FZ = frozen internal compartment ACC = accessible internal compartment C = Cdc42 concentrated BT = Cdc42 bulk traffic D = Cdc42 depleted	
Quasi–steady-state simulations	FZ_C\FZ_C_peak FZ_BT\FZ_BT_peak FZ_D\FZ_D_peak ACC_C\ACC_C_peak ACC_BT\ACC_BT_peak ACC_D\ACC_D_peak	Takes reaction-diffusion steady state as initial condition and runs the reaction diffusion + vesicle traffic model.
FRAP simulations	FZ_C\FZ_C_FRAP FZ_BT\FZ_BT_FRAP FZ_D\FZ_D_FRAP ACC_C\ACC_C_FRAP ACC_BT\ACC_BT_FRAP ACC_D\ACC_D_FRAP	Takes reaction diffusion + vesicle traffic quasi–steady state and either runs for a while before FRAP or FRAPs straight away. FRAP circle diameter determined automatically.
Traffic speed simulations	FZ_C\FZ_C_TS FZ_BT\FZ_BT_TS FZ_D\FZ_D_TS ACC_C\ACC_C_TS ACC_BT\ACC_BT_TS ACC_D\ACC_D_TS	Takes reaction-diffusion steady state as initial condition and runs the reaction diffusion + vesicle traffic model. Endocytic patches move in response to vesicle fusion/fission.

All programs (Matlab) available on request.

TABLE 2: Programs used for the simulations.

Initial conditions

Time-lapse microscopy suggests that Cdc42p polarization precedes actin polarization (Howell *et al.*, 2009). In the combined model, we started the simulations as follows:

For the plasma membrane, we initiated the simulation with the concentrations of the different species that correspond to the polarized steady state of the reaction-diffusion model without vesicles, with the polarized peak centered in the plasma membrane. The internal compartment was initiated with the Cdc42p (and in some cases GDI-Cdc42p) concentration expected for steady-state nonpolarized cells (this was different for the different trafficking scenarios). The initial cytoplasmic concentrations were calculated so as to preserve a constant total cellular Cdc42p, GDI, and Bem1p complex.

These starting conditions were intended to mimic the situation in a cell that has been unpolarized for a while (early G1) and then develops a polarized Cdc42p distribution via the reaction-diffusion mechanism, with polarized vesicle traffic about to begin. In reality, of course, some polarized vesicle traffic would begin before the reaction-diffusion system reached steady state, but in this paper we are not concerned with the very initial phase of polarity establishment.

To begin a simulation, we used the initial conditions described above as input into the relevant combined model, and the system evolved as described in *Results*.

Simulating a FRAP experiment

FRAP simulations were initiated with the polarized states reached after 1 h of simulated time, as described above. We then designated a region to be bleached. Experimentally, a microscopist designates such areas on a cell-by-cell basis with the goal of bleaching the polarized pool but leaving the rest of the cell unbleached. In practice, some additional bleaching is unavoidable, and the exact area bleached will vary slightly from cell to cell. To achieve a similar goal, we designated the area of the plasma membrane to be bleached on a simulated cell-to-cell basis. The diameter of the FRAP circle was equal to the greater of the two polarity patch diameters. Diameters ran through the center of the patch along the horizontal and vertical axes. We defined the polarity patch as the area of membrane harboring a Cdc42p concentration higher than the background level plus one micromolar. This was sufficient to capture the main body of the peak.

Bleaching. Within the designated area, all Cdc42p-containing species (i.e., GDP-Cdc42p, GDP-Cdc42p-GDI complexes, GTP-Cdc42p, and GTP-Cdc42p-Bem1p complexes) at the membrane were converted to a "dark" form. In addition, any Cdc42p-containing species in endocytic patches within the designated area were also converted. Finally, 1% of the cytoplasmic GDI-Cdc42p pool was also converted.

Recovery. After bleaching, the simulations were continued, tracking both "bleached" and "unbleached" forms of each species as the system evolved to a new state in which bleached and unbleached forms were well mixed. The amount of unbleached Cdc42p within the initially bleached area was then plotted as a FRAP curve, normalized to steady state in the deterministic, no vesicle, simulation

or to the state reached at 20 s in the vesicle-containing simulations. The choice to use the recovery at 20 s allowed direct comparison between simulation results and the experimental data reported by Slaughter *et al*. (2009; Figure 1B).

Ten FRAP curves were obtained for vesicle-containing simulations in the manner described and averaged to derive the recovery profiles shown. For simulations involving only the reaction-diffusion system (Figure 2), a single simulation was conducted, as this model lacks the stochastic noise provided by vesicle traffic.

Calculating Cdc42p fluxes. The steady state (without vesicle traffic) or polarized states after 1 h of simulated time (with vesicle traffic) of each model were used to calculate the Cdc42p fluxes to the bleached region.

GDI on-fluxes were obtained by using the steady-state GDI42c (cytoplasmic GDI-Cdc42p complex) concentration in the no-vesicles simulation or the mean GDI42c concentration averaged over 60 s in the other simulations. These concentrations were then used to calculate the GDI on-flux using the equation

$$\text{GDI on-flux} = \frac{N_F}{A_F} k_{5a} \text{GDI42c}$$

where N_F is the number of grid points in the bleached zone and A_F is the area of the bleached zone.

To calculate the vesicle-mediated on-fluxes, we first obtained the mean Cdc42p internal compartment concentrations by averaging over 60 s of simulated time. We used these values and the rate of exocytosis to calculate the expected amount of Cdc42p delivered to the membrane per second. Exocytosis only occurs within the bleached zone, so to obtain the vesicle-mediated on-fluxes, we divided the amount of Cdc42p delivered per second by the area of the bleached zone. We used the area of bleached zone from the no-vesicles simulation to calculate all fluxes, enabling direct comparison. This may slightly overestimate the vesicle-mediated on-flux, as the bleached zones in vesicle-containing simulations differ slightly due to the stochastic traffic and tend to be larger than the no-vesicle bleached zone.

Adapting the vesicle-trafficking model

One adjustment to the Layton model involves the manner in which the plasma membrane protein concentrations are redistributed immediately following vesicle fusion or fission events, which was modified in order to preserve local membrane area. The procedure is described below for fusion of an exocytic vesicle, and an analogous procedure was applied following fission of an endocytic vesicle.

We assume that points on the plasma membrane shift radially away from the vesicle fusion site. Let (x_v, y_v) be the coordinates of the center of the vesicle (Figure S2). The point at (x_0, y_0) before vesicle fusion then moves to (x_1, y_1) after vesicle fusion. For a given (x_1, y_1), we can calculate the corresponding (x_0, y_0) by making use of 1) the colinearity of (x_v, y_v), (x_0, y_0), and (x_1, y_1); and 2) the area conservation relation, $\pi r_1^2 = \pi r_0^2 + \pi r_v^2$ (Figure S2).

The coordinates (x_0, y_0) were calculated for all grid points lying within the largest circle capable of fitting in the square, simulated plasma membrane. The protein concentrations at (x_0, y_0) before insertion were estimated by linear interpolation from the nearest grid points using the Matlab "interp2" function, and then assigned to (x_1, y_1) immediately after insertion. For very distant grid points outside the circle, we assumed that any change in protein concentrations due to vesicle fusion at the center would be negligible.

Just as points are assumed to move away radially from a vesicle insertion site, we assume that the locations of endocytic patches are also radially displaced away from an exocytosis event by a distance calculated following the same scheme. Patches are displaced radially toward sites of vesicle fission using an analogous procedure. As discussed above, we assume that any patch movement at distant sites not in the largest circle capable of fitting in the square, simulated plasma membrane would be negligible.

The adjustments described above make the model more accurate, and become particularly important at high vesicle-trafficking rates. In particular, they reduce the clustering of large numbers of endocytic patches in the window, thereby avoiding the formation of endocytic patches one on top of the other. At rapid trafficking rates, there would be a significant membrane flow from the tip rearward.

Comparison of the mechanistic models to the phenomenological Slaughter model

Slaughter *et al*. analyzed their FRAP data using a mathematical model with two Cdc42p recycling pathways (mediated by GDI/diffusion and actin/vesicles), each described by a similar formalism (Slaughter *et al*., 2009). Cdc42p is delivered from an internal pool to the window, and recycled back to the internal pool from both the window and the surrounding membrane. The outward Cdc42p flux is the product of a pathway-specific rate constant (*h*) and the amount of Cdc42p in the internal pool. The return flux is the product of one of two pathway-specific rate constants (*m* in the window and *n* in the surrounding membrane) and the local concentration of Cdc42p at the membrane.

A major difference between the Slaughter model and ours is that whereas most of our parameters correspond to specific biochemical or vesicular processes, theirs do not. Thus the parameter values they derived from the data cannot directly be used to validate or discard any mechanistic hypothesis about Cdc42p trafficking.

A second difference is that we consider distinct internal pools for the GDI pathway (in which the internal pool is cytoplasmic GDI-bound Cdc42p) and the vesicle pathway (in which the internal pool is Cdc42p on an internal membrane compartment), whereas Slaughter assumed both pathways use the same internal pool.

To constrain their model and extract the rate constants, Slaughter *et al*. assumed that the shared internal pool could be measured as the summed GFP-Cdc42p fluorescence internal to the plasma membrane. We consider this unlikely to be valid, as the internal fluorescence includes distinct cytoplasmic and membrane components, and the latter include vacuolar membranes, which may not be part of a recycling endomembrane system.

In terms of the GDI pathway, Slaughter *et al*. assumed that all deposition of Cdc42p occurs in the window, whereas retrieval occurs at different rates in the window and outside the window. In contrast, we assume that deposition occurs uniformly and that retrieval is nonuniform due to variations in membrane GDP-Cdc42 concentration. In particular, GDP-Cdc42p is depleted from regions with high Bem1p complex/GEF concentration, so there is less retrieval from those regions.

In terms of the vesicle pathway, the Slaughter *et al*. assumptions are most consistent with our "bulk traffic" model, in which the amount of Cdc42p retrieved from a given location on the membrane is proportional to the Cdc42p concentration at that site. A major difference, however, is that we consider traffic of membrane as well as Cdc42p, whereas the Slaughter model considers only Cdc42p. This is important, because the "membrane-free" simplifying assumption misses critical features of the biology (Layton *et al*., 2011).

ACKNOWLEDGMENTS

We thank Nick Buchler, Meng Jin, Audrey Howell, Tim Elston, anonymous reviewers, and members of the Lew lab for comments on the manuscript. This work was funded by Public Health Service grant GM62300 to D.J.L.

REFERENCES

Araujo-Palomares CL, Richthammer C, Seiler S, Castro-Longoria E (2011). Functional characterization and cellular dynamics of the CDC-42–RAC–CDC-24 module in *Neurospora crassa*. PLoS One 6, e27148.

Ayscough KR, Stryker J, Pokala N, Sanders M, Crews P, Drubin DG (1997). High rates of actin filament turnover in budding yeast and roles for actin in establishment and maintenance of cell polarity revealed using the actin inhibitor latrunculin-A. J Cell Biol 137, 399–416.

Balch WE, McCaffery JM, Plutner H, Farquhar MG (1994). Vesicular stomatitis virus glycoprotein is sorted and concentrated during export from the endoplasmic reticulum. Cell 76, 841–852.

Bender A, Pringle JR (1989). Multicopy suppression of the cdc24 budding defect in yeast by CDC42 and three newly identified genes including the ras-related gene RSR1. Proc Natl Acad Sci USA 86, 9976–9980.

Brandman O, Ferrell JE, Jr., Li R, Meyer T (2005). Interlinked fast and slow positive feedback loops drive reliable cell decisions. Science 310, 496–498.

Chant J, Herskowitz I (1991). Genetic control of bud site selection in yeast by a set of gene products that constitute a morphogenetic pathway. Cell 65, 1203–1212.

Chant J, Pringle JR (1995). Patterns of bud-site selection in the yeast *Saccharomyces cerevisiae*. J Cell Biol 129, 751–765.

Dietrich FS *et al*. (2004). The *Ashbya gossypii* genome as a tool for mapping the ancient *Saccharomyces cerevisiae* genome. Science 304, 304–307.

Garcia-Mata R, Boulter E, Burridge K (2011). The "invisible hand": regulation of RHO GTPases by RHOGDIs. Nat Rev Mol Cell Biol 12, 493–504.

Gierer A, Meinhardt H (1972). A theory of biological pattern formation. Kybernetik 12, 30–39.

Goryachev AB, Pokhilko AV (2008). Dynamics of Cdc42 network embodies a Turing-type mechanism of yeast cell polarity. FEBS Lett 582, 1437–1443.

Harrison JC, Bardes ES, Ohya Y, Lew DJ (2001). A role for the Pkc1p/Mpk1p kinase cascade in the morphogenesis checkpoint. Nat Cell Biol 3, 417–420.

Howell AS, Jin M, Wu C-F, Zyla TR, Elston TC, Lew DJ (2012). Negative feedback enhances robustness in the yeast polarity establishment circuit. Cell 149, 322–333.

Howell AS, Savage NS, Johnson SA, Bose I, Wagner AW, Zyla TR, Nijhout HF, Reed MC, Goryachev AB, Lew DJ (2009). Singularity in polarization: rewiring yeast cells to make two buds. Cell 139, 731–743.

Irazoqui JE, Gladfelter AS, Lew DJ (2003). Scaffold-mediated symmetry breaking by Cdc42p. Nat Cell Biol 5, 1062–1070.

Jilkine A, Edelstein-Keshet L (2011). A comparison of mathematical models for polarization of single eukaryotic cells in response to guided cues. PLoS Comput Biol 7, e1001121.

Johnson JL, Erickson JW, Cerione RA (2009). New insights into how the Rho guanine nucleotide dissociation inhibitor regulates the interaction of Cdc42 with membranes. J Biol Chem 284, 23860–23871.

Johnson JM, Jin M, Lew DJ (2011). Symmetry breaking and the establishment of cell polarity in budding yeast. Curr Opin Genet Dev 21, 740–746.

Kaksonen M, Sun Y, Drubin DG (2003). A pathway for association of receptors, adaptors, and actin during endocytic internalization. Cell 115, 475–487.

Kohli M, Galati V, Boudier K, Roberson RW, Philippsen P (2008). Growth-speed-correlated localization of exocyst and polarisome components in growth zones of *Ashbya gossypii* hyphal tips. J Cell Sci 121, 3878–3889.

Kozubowski L, Saito K, Johnson JM, Howell AS, Zyla TR, Lew DJ (2008). Symmetry-breaking polarization driven by a Cdc42p GEF-PAK complex. Curr Biol 18, 1719–1726.

Layton AT, Savage NS, Howell AS, Carroll SY, Drubin DG, Lew DJ (2011). Modeling vesicle traffic reveals unexpected consequences for cdc42p-mediated polarity establishment. Curr Biol 21, 184–194.

Marco E, Wedlich-Soldner R, Li R, Altschuler SJ, Wu LF (2007). Endocytosis optimizes the dynamic localization of membrane proteins that regulate cortical polarity. Cell 129, 411–422.

Meinhardt H, Gierer A (1974). Applications of a theory of biological pattern formation based on lateral inhibition. J Cell Sci 15, 321–346.

Nomanbhoy TK, Erickson JW, Cerione RA (1999). Kinetics of Cdc42 membrane extraction by Rho-GDI monitored by real-time fluorescence resonance energy transfer. Biochemistry 38, 1744–1750.

Novick P, Field C, Schekman R (1980). Identification of 23 complementation groups required for post-translational events in the yeast secretory pathway. Cell 21, 205–215.

Orlando K, Sun X, Zhang J, Lu T, Yokomizo L, Wang P, Guo W (2011). Exo-endocytic trafficking and the septin-based diffusion barrier are required for the maintenance of Cdc42p polarization during budding yeast asymmetric growth. Mol Biol Cell 22, 624–633.

Ozbudak EM, Becskei A, van Oudenaarden A (2005). A system of counteracting feedback loops regulates Cdc42p activity during spontaneous cell polarization. Dev Cell 9, 565–571.

Prescianotto-Baschong C, Riezman H (1998). Morphology of the yeast endocytic pathway. Mol Biol Cell 9, 173–189.

Pruyne D, Legesse-Miller A, Gao L, Dong Y, Bretscher A (2004). Mechanisms of polarized growth and organelle segregation in yeast. Annu Rev Cell Dev Biol 20, 559–591.

Schmitz HP, Philippsen P (2011). Evolution of multinucleated *Ashbya gossypii* hyphae from a budding yeast-like ancestor. Fungal Biol 115, 557–568.

Shaw BD, Chung DW, Wang CL, Quintanilla LA, Upadhyay S (2011). A role for endocytic recycling in hyphal growth. Fungal Biol 115, 541–546.

Slaughter BD, Das A, Schwartz JW, Rubinstein B, Li R (2009). Dual modes of cdc42 recycling fine-tune polarized morphogenesis. Dev Cell 17, 823–835.

Turing A (1952). The chemical basis of morphogenesis. Philos Trans R Soc Lond B Biol Sci 237, 37–72.

Upadhyay S, Shaw BD (2008). The role of actin, fimbrin and endocytosis in growth of hyphae in *Aspergillus nidulans*. Mol Microbiol 68, 690–705.

Valdez-Taubas J, Pelham HR (2003). Slow diffusion of proteins in the yeast plasma membrane allows polarity to be maintained by endocytic cycling. Curr Biol 13, 1636–1640.

Wedlich-Soldner R, Altschuler S, Wu L, Li R (2003). Spontaneous cell polarization through actomyosin-based delivery of the Cdc42 GTPase. Science 299, 1231–1235.

Wedlich-Soldner R, Li R (2004). Closing the loops: new insights into the role and regulation of actin during cell polarization. Exp Cell Res 301, 8–15.

Wedlich-Soldner R, Wai SC, Schmidt T, Li R (2004). Robust cell polarity is a dynamic state established by coupling transport and GTPase signaling. J Cell Biol 166, 889–900.